Hindawi
International Journal of Antennas and Propagation
Volume 2019, Article ID 3487149, 12 pages
https://doi.org/10.1155/2019/3487149

Research Article

A Statistical Channel Model for Stochastic Antenna Inclination Angles

Gang Liu, Ming Zhang, and Yaming Bo

College of Electronic and Optical Engineering & College of Microelectronics, Nanjing University of Posts and Telecommunications, Nanjing 210003, China

Correspondence should be addressed to Yaming Bo; ymbo@njupt.edu.cn

Received 28 August 2018; Accepted 3 February 2019; Published 28 March 2019

Guest Editor: Raed A. Abd-Alhameed

The actions of a person holding a mobile device are not a static state but can be considered as a stochastic process since users can change the way they hold the device very frequently in a short time. The change in antenna inclination angles with the random actions will result in varied received signal intensity. However, very few studies and conventional channel models have been performed to capture the features. In this paper, the relationships between the statistical characteristics of the electric field and the antenna inclination angles are investigated and modeled based on a three-dimensional (3D) fast ray-tracing method considering both the diffraction and reflections, and the radiation patterns of an antenna with arbitrary inclination angles are deducted and included in the method. Two different conditions of the line-of-sight (LOS) and non-line-of-sight (NLOS) in the indoor environment are discussed. Furthermore, based on the statistical analysis, a semiempirical probability density function of antenna inclination angles is presented. Finally, a novel statistical channel model for stochastic antenna inclination angles is proposed, and the ergodic channel capacity is analyzed.

1. Introduction

Wireless communication technology has been widely used in communication systems for its mobility, convenience, flexibility, and lower cost compared with wired transmission. However, the signals are significantly affected by the surrounding environment and undergo fading and time variation before arriving at the receiver. In order to achieve a higher rate and more reliable communication, the acquisition of accurate channel state information (CSI) and channel modelling is fundamental and crucial in designing a wireless communication system and has been attracting researchers' attention.

A basic framework of the geometry-based stochastic channel modelling approach (GSCMA) is developed in [1] for three different scenarios with the corresponding channel parameters such as delay spread, angle spread, shadow fading, angle of departure, angle of arrival, and delay power spectrum extracted from a large number of measurements. Additionally, a polarized channel model is also proposed based on crosspolarization discrimination (XPD) when considering the depolarization effect of channels on electromagnetic waves. The WINNER II channel model [2] extends the number of scenarios to more than a dozen but follows the same channel modelling approach. Furthermore, the WINNER II channel model allows propagation between line-of-sight (LOS) and non-line-of-sight (NLOS) conditions for a same scenario. Analogously, a number of channel models are established using GSCMA but assuming that the scatterers are distributed on regular geometries in two or three dimensions such as the one-ring model [3], twin-cluster model [4], and elliptical model [5] considering only the azimuth angle and the double-cylinder model [6], two-sphere model [7], and multiconfocal ellipsoid model [8] considering the influence of the elevation angle. However, these conventional channel models are assumed to be generally stationary, but this is not sufficiently applicable for the channels of the massive multiple-input multiple-output (MIMO) recognized as one of the most important candidate technologies for the fifth-generation (5G) mobile communication systems due to the potential and additional advantages compared with conventional MIMO technologies [9–11].

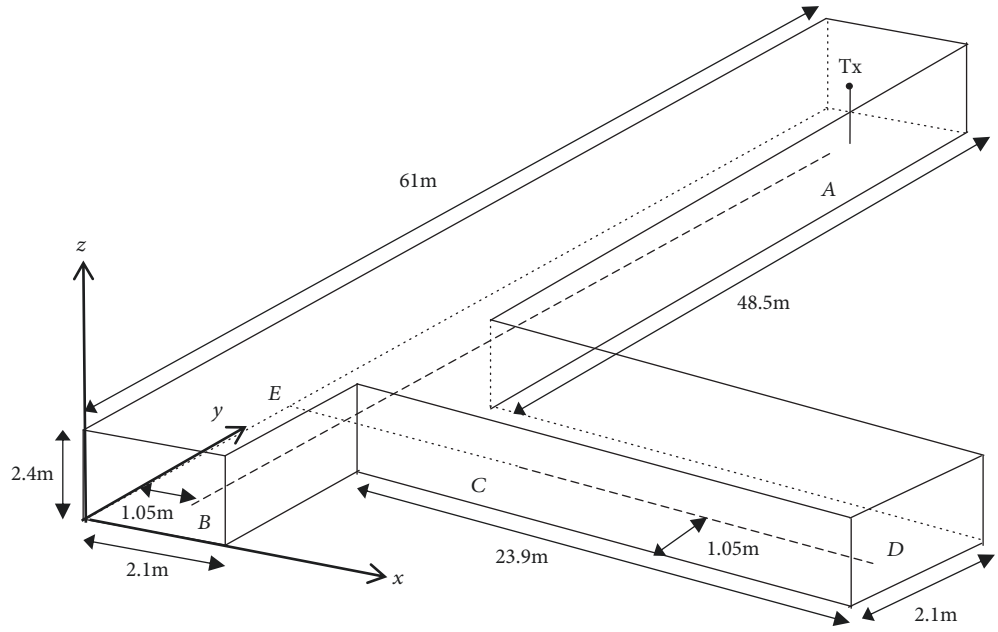

Figure 1: The three-dimensional layout of the T-shaped corridor.

Consequently, several novel models [12–14] are developed to capture the new features observed from the measurements such as the spherical wave front, nonstationary effect on the antenna array axis and the time axis.

The above channel models are independent of the antenna configurations and element radiation patterns. Instead, the correlative channel models such as the Kronecker model [15] and the Weichselberger model [16] use the correlation matrices at the mobile station (MS) and base station (BS) without knowing the distribution of scatterers or clusters resulting in a lower complexity. However, few studies of the channel modelling for stochastic antenna inclination angles have been done. It is known that mobile devices are not fixed on walls or people's desks as routers or computers. Instead, people communicate using a mobile device whenever and wherever possible; for instance, they are lying down, standing, and walking. The way people hold a mobile device is not a static state but a stochastic process since users can change the way they hold the mobile device very frequently even in a few seconds. Consequently, the antenna inclination angles will change with the rotation of the mobile devices leading to the variation of received signals due to the polarization mismatch between the signals and antennas. In this paper, a statistical channel model for stochastic antenna inclination angles in the indoor environment is developed based on a modified three-dimensional (3D) fast ray-tracing method. Two different conditions of LOS and NLOS for a common scenario of the T-shaped corridor for an indoor environment are investigated. Furthermore, in order to capture the stochastic characteristics of people holding a mobile device, a semiempirical probability density function (PDF) of antenna inclination angles is proposed, and closed expressions for the radiation patterns of a half-wave antenna for arbitrary inclination angles are deducted based on the principle of coordinate transformation. Finally, the ergodic capacities under two different conditions are analyzed based on the proposed channel model.

This paper is organized as follows. A modified 3D fast ray-tracing method is introduced, and the validity and accuracy of the method in predicting the electromagnetic fields are verified in Section II. In Section III, the statistical channel model for stochastic antenna inclination angles is presented in detail. The numerical results are analyzed in Section IV, and conclusions are drawn in Section V.

2. Simulation Environment, Method, and Validation

In this section, a modified 3D fast ray-tracing method based on space subdivision is introduced and used to predict the electromagnetic fields in a T-shaped corridor. The layout and corresponding sizes of the corridor are shown in Figure 1. It is composed of brick walls, concrete floor, and ceiling with the corresponding parameters: the relative permittivity and conductivity are $\varepsilon_r = 4.0$ and $\sigma_2 = 0.343$ s/m for the walls and $\varepsilon_r = 6.14$ and $\sigma_2 = 1.005$ s/m for the floor and ceiling [17]. If all the angles in the corridor are assumed to be right angles, the whole space of the corridor can be divided into many hexahedrons and each hexahedron can be further split into five tetrahedrons. Each hexahedron and tetrahedron must be seamless and nonoverlapping. It is worth noting that there are two different types of faces or lines in the model. One is called real face (RF) or real line (RL) since the face or line exists in the realistic scene such as the surface or edge of a wall. The other one is invisible in fact and only introduced for subsequent analyses and computations so that it is called the virtual face (VF) or virtual line (VL). The space meshing should make each face of a tetrahedron have only one property, the real or the virtual.

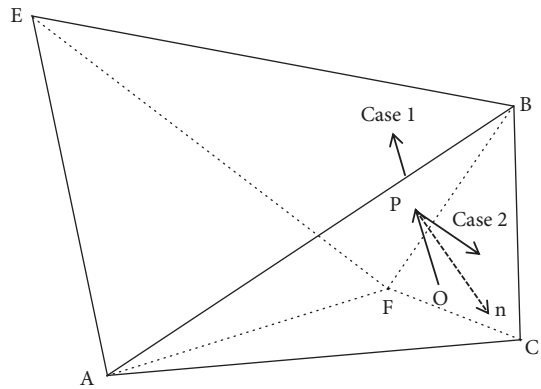

Figure 2: The demonstration of determining the next tetrahedron.

Since the size of an antenna is relatively small compared with the realistic propagation environment, a single antenna can be approximated as a transmitting point. If the coordinates of the transmitting point are given, the initial tetrahedron where the transmitting point is located in can be determined. The rays depart from the transmitting point and arrive at a receiving point through a number of tetrahedrons, and the path of each ray can be traced using the method proposed in [18]. However, the calculation is so cumbersome that we modify the expression and give a more compact form as

$$\alpha_i = \frac{\left\langle \overrightarrow{\mathrm{OB}}, \overrightarrow{n_i} \right\rangle}{\left\langle \overrightarrow{r}, \overrightarrow{n_i} \right\rangle}, \quad i = 1, 2, 3, 4, \tag{1}$$

where $\overrightarrow{\mathrm{OB}}$ denotes the vector from the transmitting point O to an arbitrary vertex of the i-th face of the initial tetrahedron as shown in Figure 2 and $\overrightarrow{n_i}$ and a_i represent the normal vector and extension coefficient of the i-th face, respectively. $\overrightarrow{r}$ is the unit vector of propagation, and $\langle \cdot, \cdot \rangle$ represents the inner product of two vectors. Consequently, the face hit by the ray corresponds to the minimum and positive extension coefficient.

Note that there are two cases of propagation for different type of faces. If the face is a VF, the incident rays will pass through the face and reach the adjacent tetrahedron as in the case 1 shown in Figure 2. Otherwise, the face is a RF, and the incident rays will be reflected in the current tetrahedron as in the case 2. If the roughness of all surfaces in the environment is assumed to be neglected, the reflected field can be determined according to Fresnel's laws of reflection. The reflection coefficients for perpendicular polarization and parallel polarization are given as

$$\Gamma_{\perp} = \frac{\cos\theta_i - \sqrt{\varepsilon_r - \sin^2\theta_i}}{\cos\theta_i + \sqrt{\varepsilon_r - \sin^2\theta_i}}, \tag{2}$$

$$\Gamma_{//} = \frac{\varepsilon_r \cdot \cos\theta_i - \sqrt{\varepsilon_r - \sin^2\theta_i}}{\varepsilon_r \cdot \cos\theta_i + \sqrt{\varepsilon_r - \sin^2\theta_i}}, \tag{3}$$

where ε_r is the relative permittivity and θ_i is the incident angle.

Furthermore, if an obstacle with the size much larger than the wavelength of the incident wave is present in the propagation path, the diffraction should be taken into consideration. In order to determine the diffraction field, Holm's heuristic diffraction coefficients are selected to calculate the diffraction field due to the simple expressions and the good consistency with the rigorous solution for finite conductivity as shown in [19]. The diffraction coefficients for perpendicular polarization and parallel polarization are expressed in a more compact form as

$$\begin{aligned} D_{//}^{\perp}\left(L, n, \varphi, \varphi'\right) = {} & \frac{-e^{-j(\pi/4)}}{2n\sqrt{2\pi k}} \cdot \left\{ \cot\left[\frac{\pi - \left(\varphi - \varphi'\right)}{2n}\right] \right. \\ & \cdot F\left[2kLn^2 \sin^2\left(\frac{\pi - \left(\varphi - \varphi'\right)}{2n}\right)\right] \\ & + R_{0_{//}^{\perp}} R_{n_{//}^{\perp}} \cot\left[\frac{\pi + \left(\varphi - \varphi'\right)}{2n}\right] \\ & \cdot F\left[2kLn^2 \sin^2\left(\frac{\pi + \left(\varphi - \varphi'\right)}{2n}\right)\right] \\ & + R_{0_{//}^{\perp}} \cot\left[\frac{\pi - \left(\varphi + \varphi'\right)}{2n}\right] \\ & \cdot F\left[2kLn^2 \sin^2\left(\frac{\pi - \left(\varphi + \varphi'\right)}{2n}\right)\right] \\ & + R_{n_{//}^{\perp}} \cot\left[\frac{\pi + \left(\varphi + \varphi'\right)}{2n}\right] \\ & \left. \cdot F\left[2kLn^2 \sin^2\left(\frac{\pi + \left(\varphi + \varphi'\right)}{2n}\right)\right] \right\}, \\ F(x) = {} & 2j\sqrt{x}e^{jx}\int_{\sqrt{x}}^{\infty} e^{-j\tau^2} d\tau, \\ L = {} & \frac{ss'}{s + s'}, \end{aligned} \tag{4}$$

where $R_{0_{//}^{\perp}}$ and $R_{n_{//}^{\perp}}$ are the reflection coefficients for the perpendicular polarization and parallel polarization referred to in the formulas expressed in (2) and (3) for the 0-face and n-face [19]. ϕ' and ϕ represent the incident angle and diffraction angle, respectively. k is the wave number, $(2 - n)\pi$ is the inner angle of the wedge and here $n = 1.5$ due to the previous assumption of right angles in the corridor, s is the distance between the diffraction point and the diffraction observation

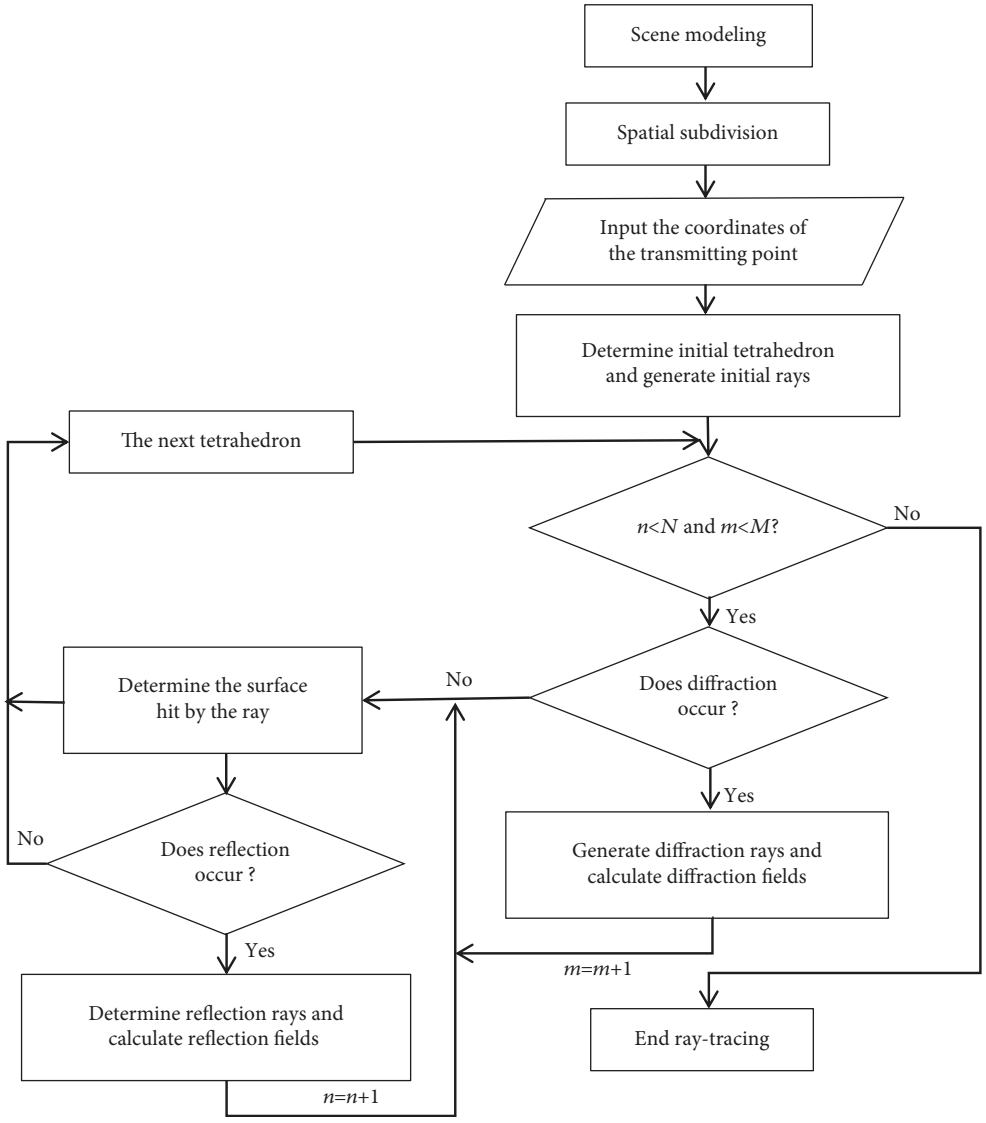

Figure 3: Flow chart of the 3D fast ray-tracing method.

point, and s' is the distance between the source point of the incident ray and the diffraction point.

The process of the 3D fast ray-tracing is shown in Figure 3, where N and M denote the number of reflections and the number of reflections after diffraction, respectively.

In the process of ray-tracing, it is assumed that each ray is independent of each other and the field around a ray should be represented only by the ray. In addition, it is necessary to determine whether a ray contributes to the field at a receiving point. One of the effective methods is using the reception sphere [20]. The radius of the reception sphere for each ray is expressed as

$$r = \frac{\alpha d}{\sqrt{3}}, \tag{5}$$

where α is the angle between two adjacent rays and d is the path length from the transmitting point to the receiving point.

Note that if the receiving point locates in the overlapping area of the rays, the double counting error [21] will be generated. A method of reducing the double count error is presented as follows.

Firstly, in order to determine whether a ray is received, all its adjacent rays need to be tested simultaneously. Secondly, if an adjacent ray is received, it must be determined whether the number of reflections and the surfaces in the whole paths of the two rays are equal. If it is true, we compare the distances from the receiving point to the two rays and discard the further one as a repeated ray. Otherwise, the two rays will be retained.

It is known that when people are communicating with mobile devices, the rapidly changing actions of holding their mobile devices result in the antenna inclination angles varying randomly. Assuming that half-wave dipole antennas are used on both the transmitting and receiving sides, and if the coordinate system of the antenna is taken as the local coordinate system and the coordinate system of the corridor

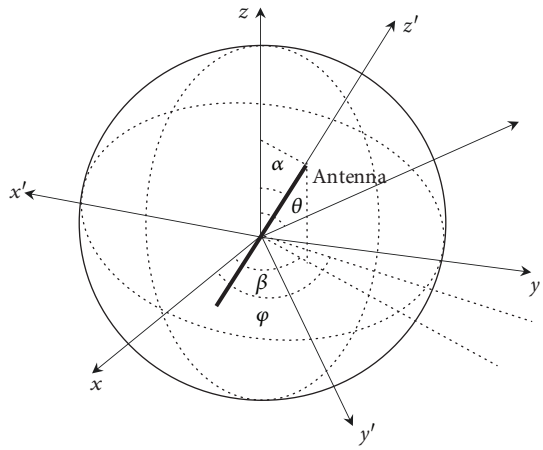

Figure 4: The demonstration of two coordinate systems. x-y-z is the global coordinate system, and x'-y'-z' is the local coordinate system.

environment is considered as the global coordinate system as shown in Figures 1 and 4, the radiation patterns of the antenna also change with the antenna inclination angles in the global coordinate system. According to the coordinate transformation, radiation patterns of a half-wave dipole antenna with arbitrary inclination angles are expressed as

$$\begin{aligned} F_\theta(\alpha,\beta,\theta,\varphi) &= (\cos\alpha\sin\theta - \sin\alpha\cos\beta\cos\theta\cos\varphi \\ &\quad - \sin\alpha\sin\beta\cdot\cos\theta\sin\varphi)\cdot\frac{\cos((\pi/2)\chi)}{1-\chi^2}, \\ F_\varphi(\alpha,\beta,\theta,\varphi) &= (\sin\alpha\sin\beta\cos\varphi - \sin\alpha\cos\beta\sin\varphi) \\ &\quad \cdot\frac{\cos((\pi/2)\chi)}{1-\chi^2}, \\ \chi &= \cos\alpha\cos\theta + \sin\alpha\cos\beta\sin\theta\cos\varphi \\ &\quad + \sin\alpha\sin\beta\sin\theta\sin\varphi, \end{aligned} \tag{6}$$

where F_θ and F_φ represent the radiation pattern of the θ direction and φ direction in the global coordinate system, respectively. As shown in Figure 4, α and β represent the zenith angle and azimuth angle of the tilted antenna in the global coordinate system, respectively. θ and φ are the zenith angle and azimuth angle in the global coordinate system, respectively. For $\alpha = 0°$, the electric field patterns are simplified to

$$\begin{aligned} F_\theta &= \frac{\cos((\pi/2)\cos\theta)}{\sin\theta}, \\ F_\varphi &= 0. \end{aligned} \tag{7}$$

These are the electric field patterns of a vertical polarized half-wave dipole antenna.

Assuming that the transmitting antenna is fixed in the vertical polarization whereas the angle of the receiving antenna varies randomly, the intensity of the electric field received by the antenna will be different at the same receiving point since only the electric field components parallel to the

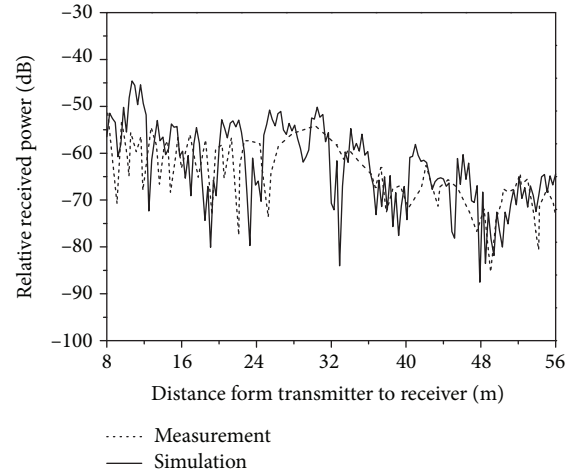

Figure 5: The relative received power from A to B in the LOS corridor ($N = 10$, $M = 8$, $G_T = 1$ dBi, and $G_R = 1$ dBi).

antenna act on the received signals. Consequently, after all the effective rays are determined, the total complex E-field can be obtained as

$$\begin{aligned} \dot{\overrightarrow{E_{\text{total}}}} = \Bigg\langle \sum_{i=1}^{K} \Bigg[& \dot{\overrightarrow{E_i}}(\theta_i,\varphi_i)\cdot\overrightarrow{e_\theta}\cdot F_\theta(\alpha,\beta,\theta_i,\varphi_i) + \dot{\overrightarrow{E_i}}(\theta_i,\varphi_i) \\ & \cdot\overrightarrow{e_\varphi}\cdot F_\varphi(\alpha,\beta,\theta_i,\varphi_i)\Bigg], \overrightarrow{S_{\text{Ant}}}(\alpha,\beta)\Bigg\rangle \cdot \overrightarrow{S_{\text{Ant}}}(\alpha,\beta), \end{aligned} \tag{8}$$

where K is the total number of the effective rays. i denotes the i-th effective subpath. $\overrightarrow{e_\theta}$ and $\overrightarrow{e_\varphi}$ are the unit direction vectors in the θ and φ directions, respectively. $\overrightarrow{S_{\text{Ant}}}$ is the antenna axial directional vector. $\langle\cdot,\cdot\rangle$ represents the inner product of two vectors. Consequently, the relative received power (RRP) (relative to transmitting power) can be obtained as [17]

$$\text{RRP(dB)} = G_T + G_R + 20\log_{10}\left|\dot{\overrightarrow{E_{\text{total}}}}\right| - \text{PL}_0, \tag{9}$$

where G_T and G_R represent the transmitting antenna gain and receiving antenna gain, respectively. PL_0 is the free space path loss from the transmitter to receiver.

In order to verify the accuracy and effectiveness of the modified 3D fast ray-tracing method used for predicting the propagation characteristics of the electromagnetic waves in the T-shaped corridor, the simulation results of RRP obtained from the method are compared with the measurement results in [17] as shown in Figures 5 and 6. The simulation using the ray-tracing method is performed at 5.3 GHz according to the configuration and parameter setting of the measurement system in [17], but the antennas are assumed to be half-wave dipole antennas at the transmitting and receiving sides. Both transmitting and receiving

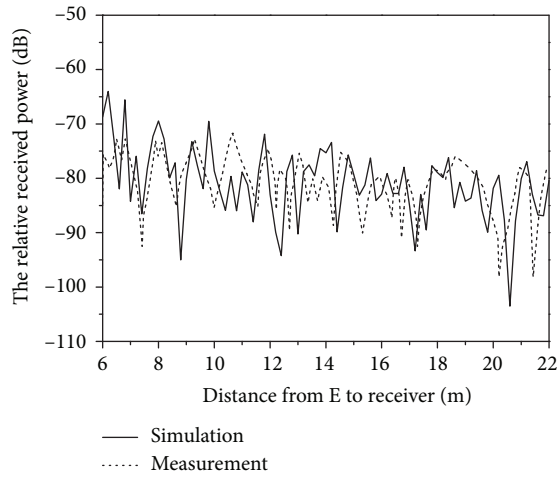

Figure 6: The relative received power from C to D in the NLOS corridor ($N = 10$, $M = 8$, $G_T = 13$ dBi, and $G_R = 1$ dBi).

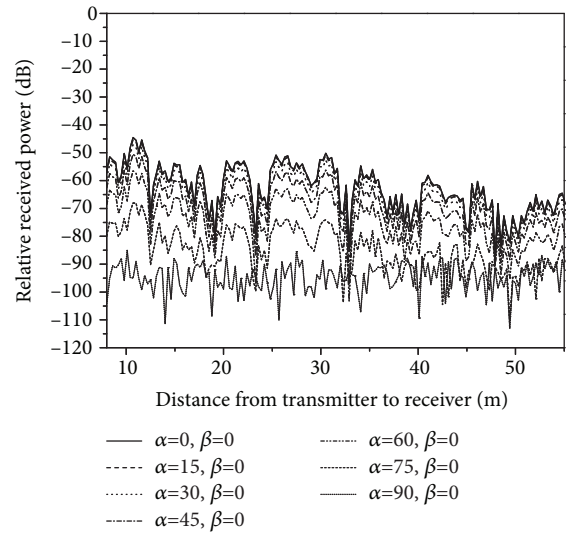

Figure 7: The relative received power for different inclination angles for the LOS corridor ($\beta = 0^\circ$, $N = 10$, $M = 8$, $G_T = 1$ dBi, and $G_R = 1$ dBi).

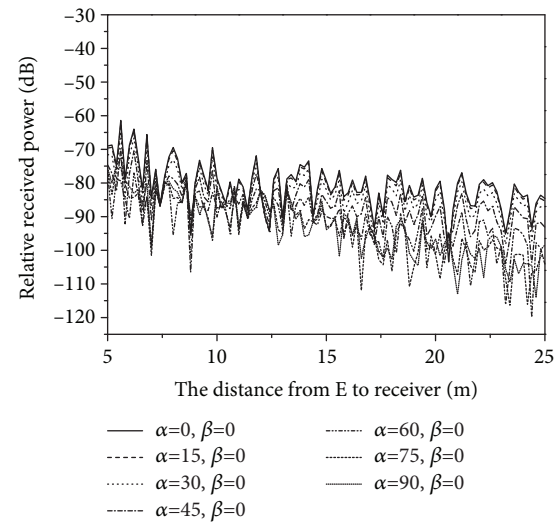

Figure 8: The relative received power for different inclination angles for the NLOS corridor ($\beta = 0^\circ$, $N = 10$, $M = 8$, $G_T = 13$ dBi, and $G_R = 1$ dBi).

antennas are vertically polarized, i.e., $\alpha = 0^\circ$. The transmitting antenna is fixed at one end of the corridor, and the receiving antenna moves along the path from points A to B in the LOS corridor and points C to D in the NLOS corridor as shown in Figure 1. The heights of the transmitting antenna and the receiving antenna are set to 1.8 m and 1.6 m, respectively. Furthermore, the transmitting power is set to be 29 dBm in the simulation, and omnidirectional vertically polarized antennas with different gains but with the same transmitting power are assumed at the transmitting side for different conditions of the LOS and NLOS corridors. As shown in Figure 5, the transmitting antenna gain and receiving antenna gain are equal to 1 dBi, i.e., $G_T = G_R = 1$ dBi, the relative received power (relative to the transmitting power) ranges from -85 dB to -45 dB and decreases along the path from points A to B in the LOS corridor as shown in Figure 1. It is known that the direct path plays a dominant role in the receiving power, and signal attenuation is mainly due to the energy diffusion and reflections on the walls, floors, and ceilings when scattering and transmission are assumed to be neglected. In another case, i.e., $G_T = 13$ dBi and $G_R = 1$ dBi, the relative received power ranges from -100 dB to -60 dB along the path from points C to D in the NLOS corridor as shown in Figure 6, and it is less than the LOS condition even for the larger transmitting antenna gain. This is because there is no direct path in the NLOS corridor, and multiple reflections and diffraction result in the heavy attenuation. The simulation results show good consistency with the measurements for both LOS and NLOS conditions even though there are some differences due to the complicated realistic corridor environment. Consequently, the method is verified to be accurate and effective in the prediction of electric field for the T-shaped corridor environment.

The intensity of the electric field received by an antenna can change with different inclination angles at a receiving point due to the polarization mismatch and the changing electric field patterns and can be analyzed using the modified 3D fast ray-tracing method. For instance, assuming the azimuth angle is equal to zero degrees, the relationships between the relative received power and the zenith angles along the paths from point A to point B in the LOS corridor and from point C to point D in the NLOS corridor are shown in Figures 7 and 8, respectively. In the LOS corridor, the relative receiving power decreases with the increase of the zenith angle, and the offsets relative to the vertically polarized antenna, i.e., $\alpha = 0^\circ$, increase but retain almost the same trend from 0 to 75 degrees. However, for the horizontally polarized antenna, i.e., $\alpha = 90^\circ$, the relative received power is far less than the vertical polarization and shows a different trend compared with others. This is because the transmitting antenna is vertically polarized and the main propagation mechanisms are the direction and reflections. The direct path plays a dominant role in the LOS corridor resulting in the relatively weaker depolarization effect.

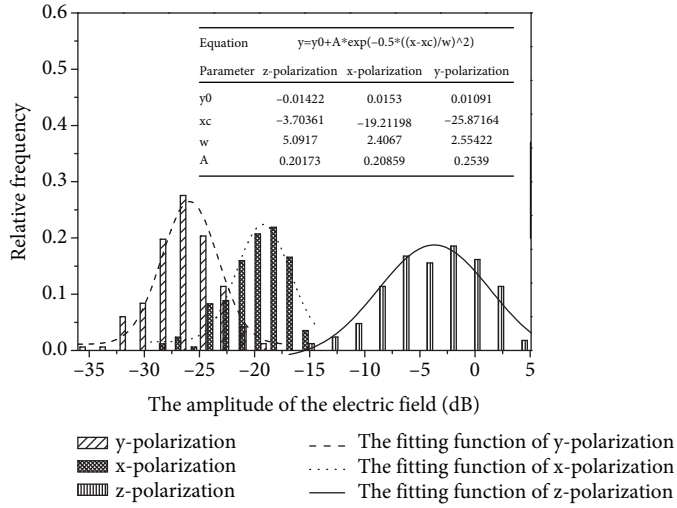

Figure 9: The probability density function (PDF) of the amplitude of the electric field in the LOS corridor.

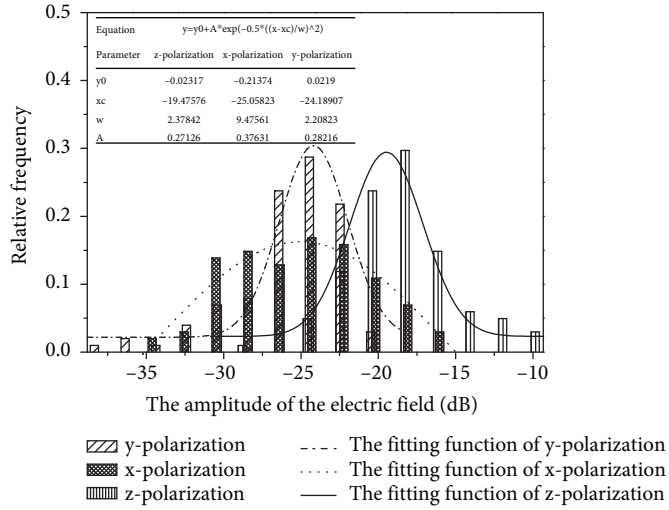

Figure 10: The probability density function (PDF) of the amplitude of the electric field in the NLOS corridor.

In the NLOS corridor, the relative received power for the vertically polarized antenna is still the largest whereas the offsets relative to the vertically polarized antenna for other angles are less than those in the LOS corridor especially for the horizontally polarized receiving antenna. This is because there is no direct path in the NLOS corridor and the main propagation mechanisms are the diffraction and reflections leading to the serious channel depolarization effect.

3. A Statistical Chanel Model for Stochastic Antenna Inclination Angles

In order to obtain the statistical CSI of the T-shaped corridor, 169 different user positions from A to B for the LOS corridor and 101 different user positions from C to D for the NLOS corridor are selected for simulation and investigation. The half-wave dipole antennas are assumed to be used at both ends of the transceiver with the transmitting power of 30 dBm, and the transmitting antenna is fixed in the vertical polarization whereas the inclination angles of the receiving antenna are variable.

The simulation results of the electric field at different receiving points can be obtained according to (8) using the ray-tracing method. According to the statistical analyses, the statistical characteristics of the amplitude and the phase of the electric field can also be obtained. The results show that the amplitude of the electric field when expressed in decibels is subject to Gauss distribution for both LOS and NLOS corridors. For instance, the statistical distribution of the amplitude of the received electric field for the vertical polarization or z-polarization, i.e., $\alpha = 0^\circ$, and two horizontal polarizations or x-polarization and y-polarization, i.e., $\alpha = 90^\circ$, $\beta = 0^\circ$, and $\beta = 90^\circ$, are shown in Figures 9 and 10. For the LOS condition, the mean value is -3.7 dB for the z-polarization and much larger than -19.2 dB for the x-polarization and -25.9 dB for the y-polarization as shown in Figure 9 since the vertical polarization and horizontal polarization are copolarized and crosspolarized relative to the transmitting antenna, respectively, and the existence

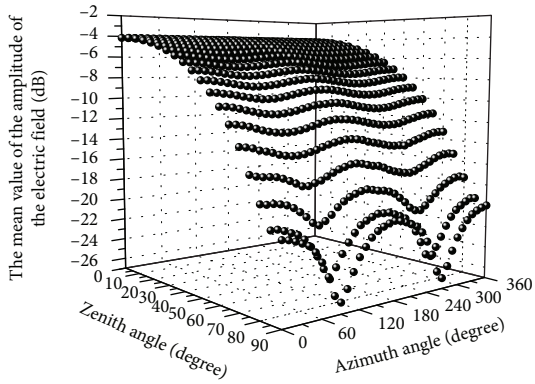

Figure 11: The mean value of the amplitude of the electric field for different inclination angles in the LOS corridor (scatter diagram).

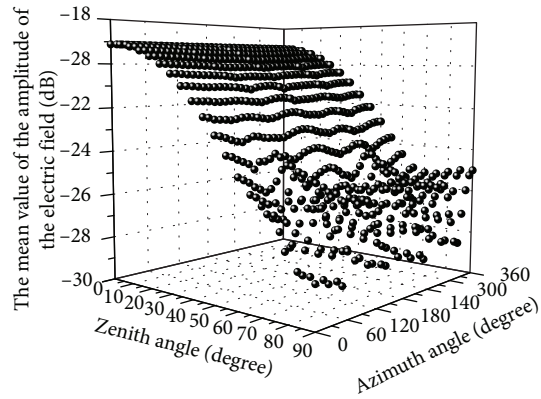

Figure 13: The mean value of the amplitude of the electric field for different inclination angles in the NLOS corridor.

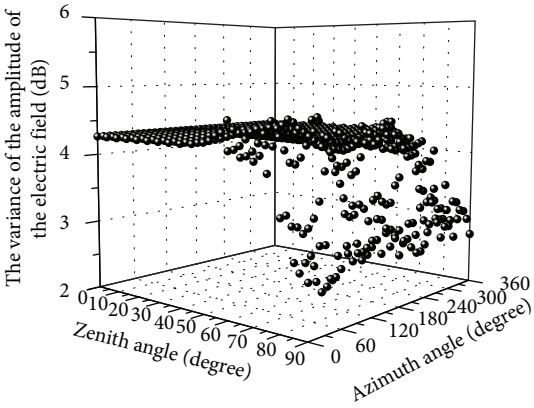

Figure 12: The variance of the amplitude of the electric field for different inclination angles in the LOS corridor (scatter diagram).

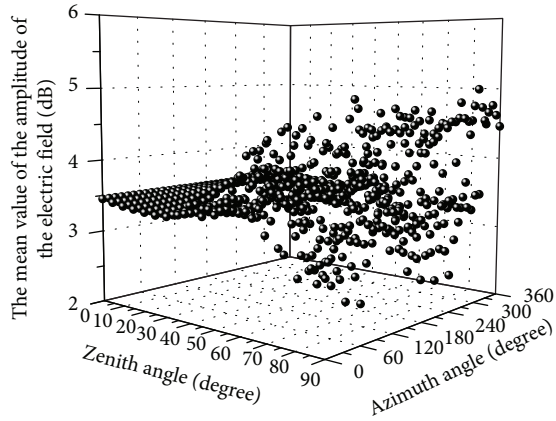

Figure 14: The variance of the amplitude of the electric field for different inclination angles in the NLOS corridor.

of the direct path leads to relatively weaker depolarization as mentioned above. Furthermore, the value of the x-polarization is larger than that of the y-polarization since the reflection surfaces in the LOS corridor are in the y direction resulting in the heavier depolarization for the component of the y-polarization than that of the x-polarization and z-polarization. For the NLOS corridor, as shown in Figure 10, the mean value is -19.5 dB for the z-polarization and approximately equal to -25 dB for the x-polarization and -24.2 dB for the y-polarization due to the strong depolarization after the diffraction and multiple reflections. Furthermore, the reflection surfaces in the NLOS corridor are in the x direction leading to nearly equal mean values of the two horizontal polarizations.

In order to obtain the statistical characteristics of received signals, the mean value and variance of the amplitude of the electric field expressed in decibels for different zenith angles and azimuth angles in the LOS corridor are depicted in Figures 11 and 12, respectively. The results show that the mean values range from -26 dB to -2 dB and decrease with the increase of the zenith angle due to the increased polarization mismatch. However, the effect of the azimuth angle is not obvious for the lower zenith angles but becomes significant for the larger zenith angles, especially when the zenith angle is equal to zero degrees; it is known that the mean value is independent of azimuth angles. This is because there are three basic polarizations as mentioned above, and the polarization mismatch also exists between two horizontal polarizations. Furthermore, the main reflection surfaces in the LOS corridor are in the y direction, which results in the heavier depolarization for the y-polarization than that of the x-polarization. However, the variance approximates to a constant of 4.25 dB for the lower zenith angles, but fluctuations occur for the larger angles as shown in Figure 12.

In the NLOS corridor, the mean values and variances of the amplitude of the electric field changing with antenna inclination angles are shown in Figures 13 and 14, respectively. The mean values range from -30 dB to -19 dB and are smaller than those of the LOS condition due to the heavy attenuation after the diffraction and multiple reflections. The depolarization transforms more power from the copolarization components into the crosspolarization ones. In addition, since the main reflection surfaces in the NLOS corridor are in the x direction, the gaps among three polarizations are reduced. Similar to the LOS condition, the variance also

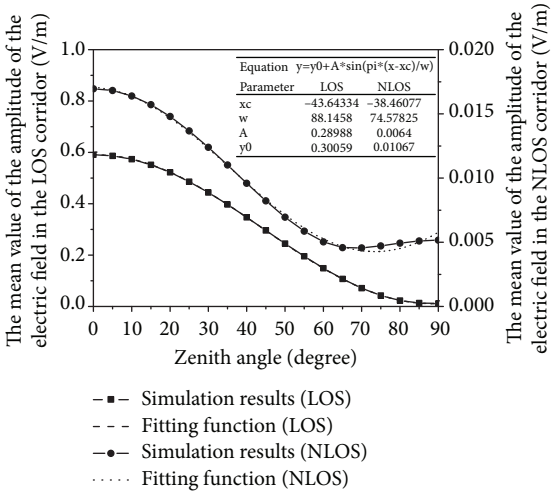

Figure 15: The mean value of the amplitude of the electric field for different inclination angles in the LOS and NLOS corridors ($\beta = 0^\circ$).

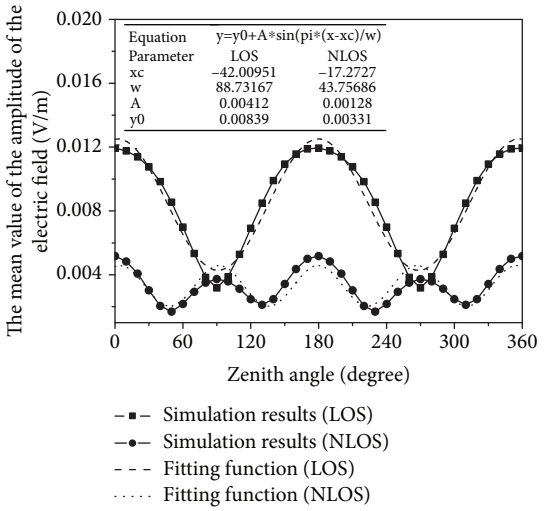

Figure 16: The mean value of the amplitude of the electric field for different inclination angles in the LOS and NLOS corridors ($\alpha = 90^\circ$).

tends to be a constant for the lower zenith angles with the value of 3.5 dB but shows approximately uniform distribution between 2.5 dB and 5 dB for the larger zenith angles.

According to the fitting results, the mean value of the amplitude of the electric field shows sinusoidal variation with the zenith angle or azimuth angle for both LOS and NLOS corridors as shown in Figures 15 and 16, and the fitting function can be expressed as

$$y = y_0 + A \sin\left(\frac{\pi(x - x_c)}{w}\right), \tag{10}$$

where y_0, A, x_c, and w are the coefficients of the fitting function. Consequently, the functional relationship between the mean value of the amplitude of the electric field and antenna inclination angles can be deducted and expressed in decibels as follows.

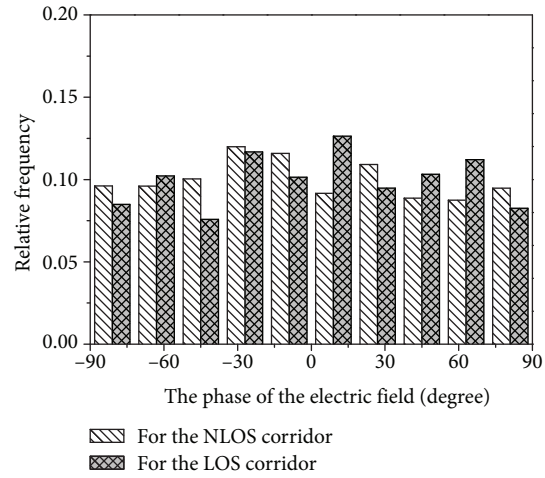

Figure 17: The statistical distribution of the phase of the electric field for the LOS and NLOS corridors.

For the LOS condition:

$$A_{\text{mean-LOS}}(\alpha, \beta) = 10 \log_{10}\left\{A_{\text{LOS}} \sin\left[\frac{\pi(\alpha - x_{c,\text{LOS}})}{w_{\text{LOS}}}\right] + 0.1976\right\}, \quad 0^\circ \le \alpha \le 90^\circ, 0^\circ \le \beta \le 360^\circ,$$
$$A_{\text{LOS}} = 0.0025 \sin(0.0357\beta - 1.7263) + 0.1902,$$
$$w_{\text{LOS}} = 0.9540 \sin(0.0356\beta - 2.009) + 88.3722,$$
$$x_{c,\text{LOS}} = 2.2633 \sin(0.0351\beta + 1.4202) - 45.474. \tag{11}$$

For the NLOS condition:

$$A_{\text{mean-NLOS}}(\alpha, \beta) = 10 \log_{10}\left\{A_{\text{NLOS}} \sin\left[\frac{\pi(\alpha - x_{c,\text{NLOS}})}{w_{\text{NLOS}}}\right] + y_{\text{NLOS}}\right\}, \quad 0^\circ \le \alpha \le 90^\circ, 0^\circ \le \beta \le 360^\circ,$$
$$A_{\text{NLOS}} = 0.0003 \sin(0.0702\beta - 1.589) + 0.0052,$$
$$x_{c,\text{NLOS}} = -42.5295 + 2.6605 \sin(0.0384\beta + 0.7388),$$
$$w_{\text{NLOS}} = 81.103 + 3.7265 \sin(0.037\beta - 1.85),$$
$$y_{\text{NLOS}} = 0.0072 + 0.0004 \sin(0.0696\beta - 4.7047). \tag{12}$$

where α and β represent the zenith angle and azimuth angle of the tilted antenna as shown in Figure 4.

According to the statistical analysis, as shown in Figure 17, the phase of the electric field is subject to uniform distribution between -90° and 90° for both LOS and NLOS corridors.

A statistical channel model for stochastic antenna inclination angles can be established as

$$H_{M_R \times N_T} = A(\alpha, \beta) \exp(j\Phi(\alpha, \beta)), \tag{13}$$

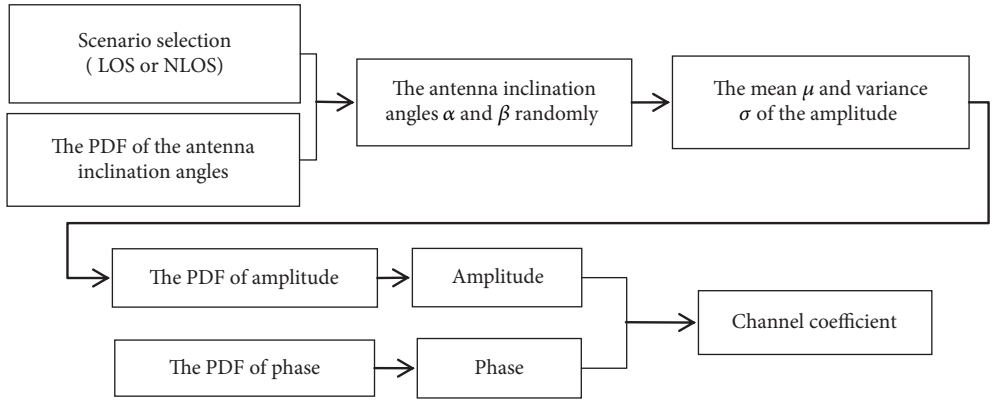

Figure 18: The flow chart of the process of generating channel coefficients.

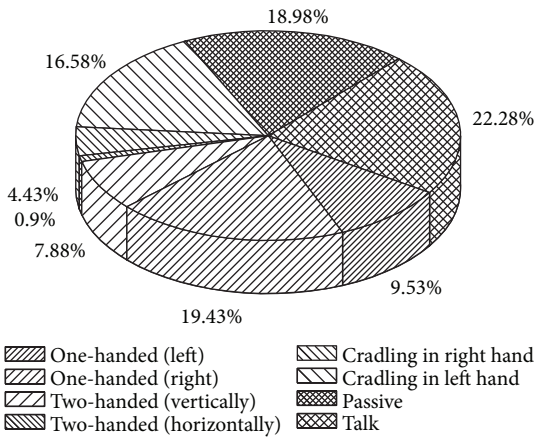

Figure 19: The pie chart of the survey results for people holding their mobile devices.

Table 1: The relationship between the way of holding the mobile devices and the antenna inclination angles.

The ways of holding the mobile devices	The antenna inclination angles (zenith angle)
Talk	0°-30°
One-handed use, two-handed use (vertically), cradling	30°-60°
Two-handed use (horizontally), passive	60°-90°

where $H_{M_R \times N_T}$ is the $M_R \times N_T$ channel matrix, M_R and N_T are the number of antennas at the transmitting and receiving sides, respectively. A and Φ represent the amplitude and phase of the channel impulse response, respectively. α and β represent the zenith angle and azimuth angle as shown in Figure 4, respectively. j is the square root of -1.

The process for generating channel coefficients is described as follows. Firstly, select the simulation scenario including the LOS or NLOS conditions and randomly generate the inclination angle of the antenna. Based on the obtained antenna inclination angles, the mean value of the amplitude of the channel coefficient for these angles can be obtained from (11) and (12). For simplicity, the variance is considered to be a constant 4.25 dB for the LOS condition or 3.5 dB for the NLOS condition as shown in Figures 12 and 14. Consequently, the amplitude of the channel coefficient is randomly generated according to the statistical distribution. Furthermore, the phase factor can also be generated in a similar way. Finally, the channel coefficient can be obtained, and the flow chart of the process for generating channel coefficients is shown in Figure 18.

4. Numerical Analysis

As mentioned above, the changing actions for people holding their mobile devices result in random variation for the antenna inclination angles. In fact, it is not a static state but can be considered as a stochastic process since it may change frequently even in a very short time. However, very few studies have been performed on the statistical characteristics of the way people hold their mobile devices. Additionally, the effect of the stochastic antenna inclination angles on received signals has not been taken into account in conventional channel models.

In [22], an interesting study of the way that people naturally hold and interact with their mobile devices is performed and 1333 observations of people using mobile devices in different situations at different places in seven cities are made. The pie chart of the survey result is shown in Figure 19. It shows that talking in the way of voice calls occupies 22.28% of the users, while 18.98% is passive activities such as listening to audio or watching a video. Furthermore, the most common way of holding the mobile devices is the one-handed use accounting for 28.96% including 67% of right-handed use and 33% of left-handed use. The 21.01% of users is engaged in cradling their mobile devices in the left hands or right hands with 79% and 21%, respectively. However, only 8.78% is two-handed use with two different situations. The first one accounting for 90% is to hold the mobile devices vertically, i.e., in the portrait mode, and the other one is to hold the mobile devices horizontally, i.e., in the landscape mode.

Although the data in [22] were used to evaluate how people actually use their mobile phones, we can empirically associate these data with the antenna inclination angles as

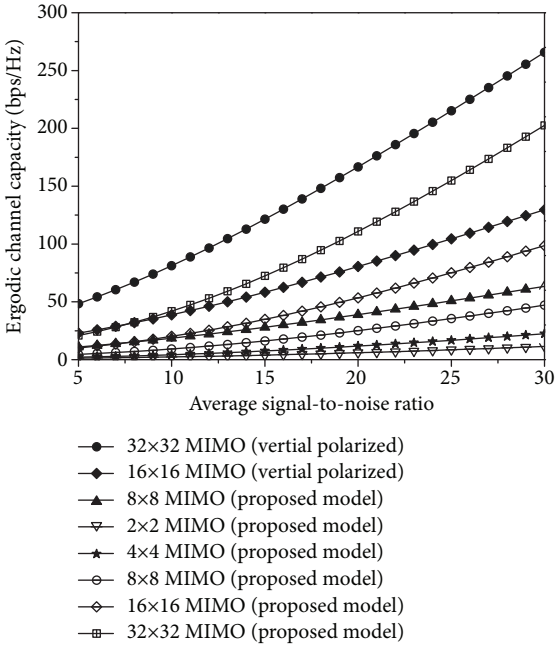

Figure 20: The ergodic channel capacity for the LOS condition.

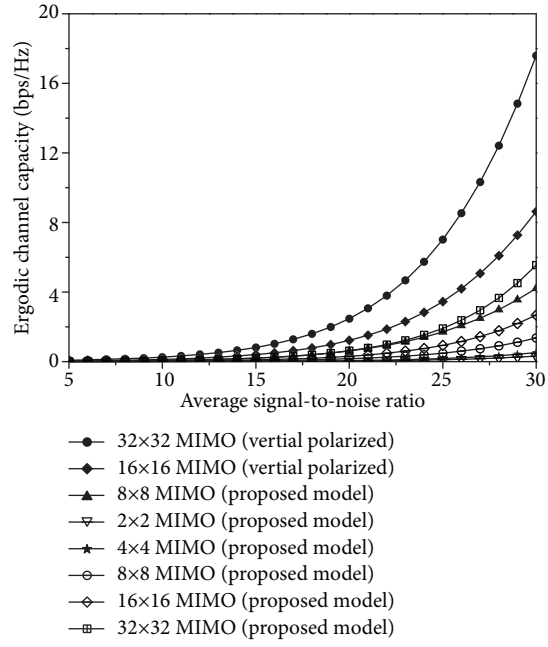

Figure 21: The ergodic channel capacity for the NLOS condition.

shown in Table 1. Consequently, a semiempirical PDF is proposed based on the survey results. According to the statistical results, the antenna inclination angle obeys Gauss distribution with the corresponding mean and standard deviation of 45.5° and 9.44°, respectively.

After obtaining the statistical distribution of antenna inclination angles, the channel coefficients can be generated according to the method introduced in Section III. In order to evaluate the channel model, taking the MIMO system of $M_T = M_R = 4$ as an example, the ergodic capacity for MIMO channels can be obtained according to the formula [23]

$$C = E\left\{\log_2 \det\left[I_{M_R} + \frac{\rho}{M_T}\mathrm{HH}^{\mathrm{H}}\right]\right\}\text{bps/Hz}, \quad (14)$$

where I_{M_R} is the $M_R \times M_R$ identity matrix; ρ is the system signal-to-noise ratio (SNR); $(\cdot)^{\mathrm{H}}$ is the Hermitian transpose; M_R and M_T denote the number of receivers and transmitters, respectively; and H is a matrix whose entries are the $M_R \times M_T$ channel gains.

The ergodic channel capacity of two different conditions of LOS and NLOS is depicted in Figures 20 and 21. The results show that the ergodic capacity increases with the increase of average SNR and it is larger in the LOS condition compared with the NLOS channel under the same SNR. Furthermore, the ergodic channel capacity increases with the increase of the number of antennas at the transmitting and the receiving sides, and for the same number of antennas, the channel capacity of the channel model with stochastic antenna inclination angles is considered to be smaller than that of the antenna fixed as a vertical polarization due to the effect of the polarization mismatch.

5. Conclusion

A 3D statistical channel model for stochastic antenna inclination angles in a T-shaped corridor environment based on a modified 3D fast ray-tracing method has been proposed in this paper. The radiation patterns for arbitrary inclination angles of a half-wave antenna have been deducted and considered in the method. Based on the statistical analyses, the relationships between the statistical characteristics of the electric field and antenna inclination angles are analyzed for both of the LOS and NLOS corridors. Furthermore, a semiempirical probability density function of antenna inclination angles has been proposed and used to depict the stochastic process of people holding their mobile devices. For future work, the channel model can serve as a preliminary attempt; the parameters used in the channel model can be verified and extracted from the channel measurements and extended to more scenarios. Combined with the existing channel models, a more general, accurate, and low-complexity channel model may be developed and applied to the next-generation wireless communication systems.

Data Availability

The data used to support the findings of this study are available from the corresponding author upon request.

Conflicts of Interest

The authors declare that they have no conflicts of interest.

Acknowledgments

This work is supported by the National Natural Science Foundation of China (NSFC) grant no. 61427801 and the Postgraduate Research & Practice Innovation Program of Jiangsu Province grant no. KYCX18_0861.

References

[1] 3GPP, *3rd Generation Partnership Project; Technical Specification Group Radio Access Networks; Spatial Channel Model for MIMO Simulations (Release 6)*, Tech. Rep. 3GPP TR 25.996 V6.1.0, 2003.

[2] IST-4-027756 WINNER II D111, *WINNER II Interim Channel Models, v1.0*, WINNER, 2006.

[3] M. Pätzold and B. O. Hogstad, "A space-time channel simulator for MIMO channels based on the geometrical one-ring scattering model," *Wireless Communications and Mobile Computing*, vol. 4, no. 7, 737 pages, 2004.

[4] H. Hofstetter, A. F. Molisch, and N. Czink, "A twin-cluster MIMO channel model," in *2006 First European Conference on Antennas and Propagation*, Nice, France, 2006.

[5] M. Pätzold and B. O. Hogstad, "A wideband MIMO channel model derived from the geometric elliptical scattering model," in *2006 3rd International Symposium on Wireless Communication Systems*, Valencia, Spain, 2006.

[6] R. He, G. L. Stüber, B. Ai, and Z. Zhong, "A two-cylinder based polarized MIMO channel model," in *2017 XXXIInd General Assembly and Scientific Symposium of the International Union of Radio Science (URSI GASS)*, Montreal, QC, Canada, 2017.

[7] Y. Yuan, X. Cheng, C. X. Wang, D. I. Laurenson, X. H. Ge, and F. Zhao, "Space-time correlation properties of a 3D two-sphere model for non-isotropic MIMO mobile-to-mobile channels," in *2010 IEEE Global Telecommunications Conference GLOBECOM*, Miami, FL, USA, 2010.

[8] L. Bai, C. X. Wang, S. B. Wu, J. Sun, and W. S. Zhang, "A 3-D wideband multi-confocal ellipsoid model for wireless massive MIMO communication channels with uniform planar antenna array," in *2017 IEEE 85th Vehicular Technology Conference (VTC Spring)*, Sydney, NSW, Australia, 2017.

[9] E. G. Larsson, O. Edfors, F. Tufvesson, and T. L. Marzetta, "Massive MIMO for next generation wireless systems," *IEEE Communications Magazine*, vol. 52, no. 2, pp. 186–195, 2014.

[10] F. Rusek, D. Persson, Buon Kiong Lau, E. G. Larsson, T. L. Marzetta, and F. Tufvesson, "Scaling up MIMO: opportunities and challenges with very large arrays," *IEEE Signal Processing Magazine*, vol. 30, no. 1, pp. 40–60, 2013.

[11] L. Lu, G. Y. Li, A. L. Swindlehurst, A. Ashikhmin, and R. Zhang, "An overview of massive MIMO: benefits and challenges," *IEEE Journal of Selected Topics in Signal Processing*, vol. 8, no. 5, pp. 742–758, 2014.

[12] S. Wu, C.-X. Wang, H. Haas, e.-H. M. Aggoune, M. M. Alwakeel, and B. Ai, "A non-stationary wideband channel model for massive MIMO communication systems," *IEEE Transactions on Wireless Communications*, vol. 14, no. 3, pp. 1434–1446, 2015.

[13] S. Wu, C.-X. Wang, e.-H. M. Aggoune, M. M. Alwakeel, and Y. He, "A non-stationary 3-D wideband twin-cluster model for 5G massive MIMO channels," *IEEE Journal on Selected Areas in Communications*, vol. 32, no. 6, pp. 1207–1218, 2014.

[14] K. Zheng, S. Ou, and X. Yin, "Massive MIMO channel models: a survey," *International Journal of Antennas and Propagation*, vol. 2014, Article ID 848071, 10 pages, 2014.

[15] J. P. Kermoal, L. Schumacher, K. I. Pedersen, P. E. Mogensen, and F. Frederiksen, "A stochastic MIMO radio channel model with experimental validation," *IEEE Journal on Selected Areas in Communications*, vol. 20, no. 6, pp. 1211–1226, 2002.

[16] W. Weichselberger, M. Herdin, H. Özcelik, and E. Bonek, "A stochastic MIMO channel model with joint correlation of both link ends," *IEEE Transactions on Wireless Communications*, vol. 5, no. 1, pp. 90–100, 2006.

[17] X. Zhao, S. Geng, L. Vuokko, J. Kivinen, and P. Vainikainen, "Polarization behaviours at 2, 5 and 60 GHz for indoor mobile communications," *Wireless Personal Communications*, vol. 27, no. 2, pp. 99–115, 2003.

[18] Z. Zhang, Z. Yun, and M. F. Iskander, "3D tetrahedron ray tracing algorithm," *Electronics Letters*, vol. 37, no. 6, pp. 334-335, 2001.

[19] P. D. Holm, "A new heuristic UTD diffraction coefficient for nonperfectly conducting wedges," *IEEE Transactions on Antennas and Propagation*, vol. 48, no. 8, pp. 1211–1219, 2000.

[20] S. Y. Seidel and T. S. Rappaport, "Site-specific propagation prediction for wireless in-building personal communication system design," *IEEE Transactions on Vehicular Technology*, vol. 43, no. 4, pp. 879–891, 1994.

[21] G. Durgin, N. Patwari, and T. S. Rappaport, "An advanced 3D ray launching method for wireless propagation prediction," in *1997 IEEE 47th Vehicular Technology Conference. Technology in Motion*, pp. 785–789, Phoenix, AZ, USA, 2002.

[22] S. Hoober, *How do people really hold and touch their mobile devices*, Online Forums, 2013.

[23] G. J. Foschini and M. J. Gans, "On the limits of wireless communications in a fading environment when using multiple antennas," *Wireless Personal Communications*, vol. 6, no. 3, pp. 311–335, 1998.